Phys. Status Solidi A **212**, No. 3, 573–578 (2015) / **DOI** 10.1002/pssa.201431703

physica status solidi a
www.pss-a.com
applications and materials science

Directional growth of nanocrystalline Si nanorod array by mid-frequency magnetron sputtering

Junhua Gao[1], Liang Wu[1], Chengjun Tu[1], Hongtao Cao[*,1], and Aiping Jin[2]

[1] Division of Functional Materials and Nano Devices, Ningbo Institute of Materials Technology and Engineering, Chinese Academy of Sciences, Ningbo 315201, P. R. China
[2] School of Chemistry and Chemical Engineering, Wuhan Textile University, Wuhan 40073, P. R. China

Received 21 August 2014, revised 14 October 2014, accepted 14 October 2014
Published online 6 November 2014

Keywords growth modes, mid-frequency magnetron sputtering, nanocrystalline silicon, nanorods, pulsed bias technique

* Corresponding author: e-mail h_cao@nimte.ac.cn, Phone: +86 (0)574 86685161, Fax: +86 (0)574 86685163

A new route to fast prepare well-aligned nanocrystalline Si nanorod array by mid-frequency (MF) magnetron sputtering was proposed in this study. Pulsed bias technique has been employed to adjust ion-bombardment condition over the growing film surface. For the Si samples deposited on the glass substrates with bipolar pulsed DC power supply, it was found that the two-dimensional growth mode of Si films was converted to the one-dimensional growth pattern at negative bias voltages no less than −60 V. The growth mode transition was ascribed to the coarsening of the growing surface in conjunction with atomic-scale shadowing effect. The nanocrystalline Si nanorods were also fabricated on stainless steel substrates successfully.

© 2014 WILEY-VCH Verlag GmbH & Co. KGaA, Weinheim

1 Introduction Compared with amorphous silicon, nanocrystalline silicon (nc-Si) is a promising material for large-area optoelectronic applications, owing to its higher carrier mobility, better stability under sunlight soaking, and more efficient absorption of long wavelength photons [1–3]. For one-dimensional nc-Si nanostructures, e.g., nanorods or nanowires, their unique structures can boost light trapping and carrier transport, leading to more prominent light absorption and carrier collection with respect to two-dimensional nc-Si thin films [4–6]. Up to now, one-dimensional silicon nanostructures have been successfully prepared by various chemical or physical methods, such as chemical vapor deposition (CVD), laser ablation, vapor–liquid–solid (VLS), sputtering, e-beam evaporation, etc. Among these techniques, magnetron sputtering or e-beam evaporation combined with glancing angle deposition (GLAD) mode has been reported to be superior to fabricate Si nanorods because of non-toxic, efficient, and easy to design and sculpt the nanorod structures by adjusting the oblique angle and the substrate rotation [7–9]. However, the silicon nanorods prepared by the above-mentioned method are almost amorphous. In addition, in order to generate the desired atomic scale shadow effect in the GLAD mode, it is necessary to set a certain large angle (>80°) between the incidence direction of sputtered atoms and the substrate normal (namely the above-stated oblique angle) [9], which would lead to the substantial loss of the deposition rate. Therefore, new routes which can speed up large-area nc-Si nanorods fabrication process are urgent whether for fundamental research or for practical application in the future.

In the mid-frequency (MF) magnetron sputtering system, one of the magnetrons acts as a sputter cathode and meanwhile the other operates as an anode at any time, resulting in high deposition rate and excellent process stability for the semiconductive films. Based upon our previous work [10] on the preparation of nc-Si thin films using an external magnetic field assisted MF unbalanced magnetron sputter system, well-aligned nc-Si nanorods on glass substrates were successfully obtained only by introducing a home-made pulsed direct current bias into the existing system. We demonstrated that the microstructure of nc-Si nanorods could be sensitively tailored by the pulsed direct current bias. Moreover, nc-Si nanorods were also fabricated on stainless steel by an appropriate substrate temperature and pulsed bias control.

© 2014 WILEY-VCH Verlag GmbH & Co. KGaA, Weinheim

2 Experimental The deposition processes were carried out by an external magnetic field-assisted MF twin magnetron sputter system, as described elsewhere [10]. The dimension of each rectangular polycrystalline silicon target is 270 mm × 70 mm, and its purity is more than 99.9995% with a resistivity of 0.2 Ω cm. A home-made pulsed direct current power supply, with three output modes (DC, unipolar pulse and bipolar pulse), was connected to the floating substrate holder as the bias supply. This power supply is capable of providing stable output with the frequency less than 100 kHz when it works in a pulsed mode. The duty cycle was fixed to be 65 and 50% for the unipolar and bipolar pulsed-bias assisted deposition, respectively. In addition, the bipolar-pulsed bias was implemented at a constant positive pulsed voltage of 10 V. Figure 1a and b shows the typical unipolar (with a frequency of 66 kHz) and bipolar (with a frequency of 10 kHz) pulsed voltage waveforms, respectively, recorded by a digital oscilloscope (Model TDS2000C, Tektronix). Since the pulsed direct current bias is one of the crucial factors for directly depositing Si nanorods, all samples in this study were prepared only by changing bias (except for depositions on stainless steel) while maintaining the other deposition parameters constant. The sputtering pressure and averaged target power density was 0.6 Pa and 1 W cm^{-2}, respectively. The substrate temperature was fixed at 510 °C while setting a coil current of 5.5 A to generate the external magnetic field. The deposition time was kept at 30 min. Prior to film growth, a pre-deposition process was carried out in order to eliminate the contaminant layer.

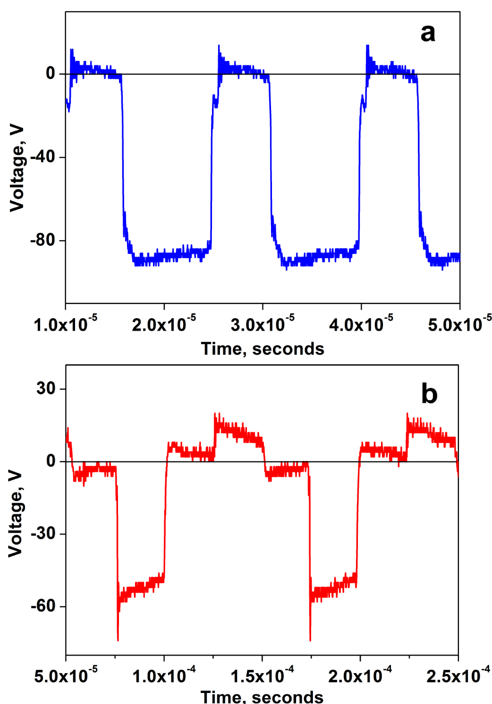

Figure 1 The typical unipolar (a) and bipolar (b) pulsed voltage waveforms with a frequency of 66 kHz (a) and 10 kHz (b), respectively.

The phase identification of samples was performed using X-ray diffraction (XRD) at a glazing incidence angle of 2°. Raman scattering spectra were collected using a JY Labram HR800 Raman spectrometer with a laser-wavelength of 632.8 nm, in order to evaluate the crystalline volume fraction (X_c) of the deposited samples. The surface and cross-sectional morphologies of the specimens were examined using scanning electron microscopy (SEM). Moreover, the microstructure of the films was also characterized by using transmission electron microscopy (TEM) technique.

3 Results and discussion The samples deposited under a floating potential or a −60 V DC bias are continuous and smooth, as shown in Fig. 2a and b, respectively. There is no clear difference whether for the film topography or their crystalline volume fractions (see Fig. 2a, b, and h), in line with the previous report [11]. For quantitatively estimating the crystalline volume fraction, the Raman spectrum in Fig. 2h was deconvoluted into two independent peaks: a broad peak at around 470–480 cm^{-1} and a sharp peak at 510–520 cm^{-1}, corresponding to the transverse optical (TO) modes of the amorphous phase ($I_{470–480}$) and the nanocrystal phase ($I_{510–520}$), respectively. Subsequently, the crystalline volume fraction X_c is defined as

$$X_c = \frac{I_{510–520}}{(I_{470–480} + I_{510–520})}. \quad (1)$$

Figure 2c and d shows the surface morphology of the samples prepared under unipolar or bipolar pulsed bias, respectively. It should be noted that the pulsed bias is operated at the same bias voltage of −60 V with an identical frequency of 10 kHz. Typical agglomerate structure with uniform size distribution over the both sample surfaces was observed, but nevertheless, the agglomerate size of the specimen deposited under the bipolar-pulsed bias is relatively larger than that of sample under the unipolar working mode. The cross-sectional images of the above two samples (Fig. 2f and g) present a clear and well-aligned columnar structure, especially for the sample shown in Fig. 2g. It was considered that the columnar structure corresponds to silicon nanorods with 50 nm in diameter, and the agglomerates are the termination of the columnar structure. The nominal deposition rate of the nanorods was ~24 nm min^{-1}. Compared with the samples prepared under DC bias, it was clearly observed that pulsed bias did play an important role in converting the growth behavior of the silicon films.

According to the previous observations, it was suggested that the ion bombardment condition close to the substrate surface can be distinctly modulated by the pulsed DC bias, resulting in the growth mode conversion. It is well known that the glass substrate, possessing a poor electrical conductivity, can be regarded as a parallel plate capacitor during the deposition processes, as qualitatively described in Fig. 4a. The surface of the glass, facing the plasma, is treated

© 2014 WILEY-VCH Verlag GmbH & Co. KGaA, Weinheim

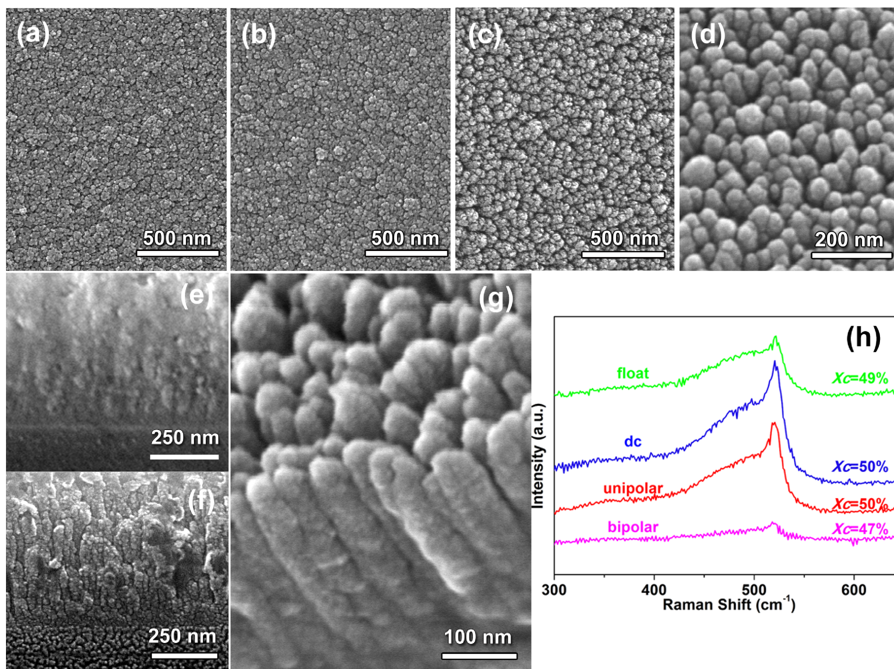

Figure 2 Surface and cross-sectional morphologies of nanocrystalline Si films or nanorods under various bias conditions: (a) floating, (b and e) DC bias, (c and f) unipolar pulsed bias, (d and g) bipolar pulsed bias, and their corresponding Raman spectra (h). The crystalline volume fraction is marked in the corresponding curves in (h).

as one plate for the capacitor, with the holder as the other. When the DC bias was loaded into the capacitor, ion flux from the plasma would quickly charge up the glass surface, i.e., a so-called charge accumulation effect. This effect would reduce the electric potential difference between the glass surface and the plasma and then attenuate the ion bombardment. Therefore, the bombardment condition near the glass substrate surface is unable to be controlled only using the DC bias. It is believed that the pulsed DC bias sputtering technique could eliminate the accumulation effect and optimize ion bombardment over the growing film even on the insulating substrate [12]. As for the columnar structure displayed in Fig. 2, it was ascribed to the enhanced atomic transport caused by intensive ion-bombardment. Furthermore, the bipolar pulsed bias is more effective to inhibit the charge build-up on the insulating substrate surface than the unipolar pulsed case [13], resulting in more prominent columnar aggregates, as displayed in Fig. 2d. More importantly, we proposed that the formation of silicon nanorods was also stemmed from the atomic-scale shadowing effect, which is due to the combinations between the rapid sputter-deposition condition and dual-target sputtering geometry [10]. In addition, the crystalline volume fraction for the bipolar-pulsed bias-fabricated sample was slightly reduced to around 47% (see Fig. 2h), implying that the excessive ion-bombardment is unfavorable to the crystallization of Si nanocrystals. Figure 3 shows the plan-view TEM images with different magnifications for the sample

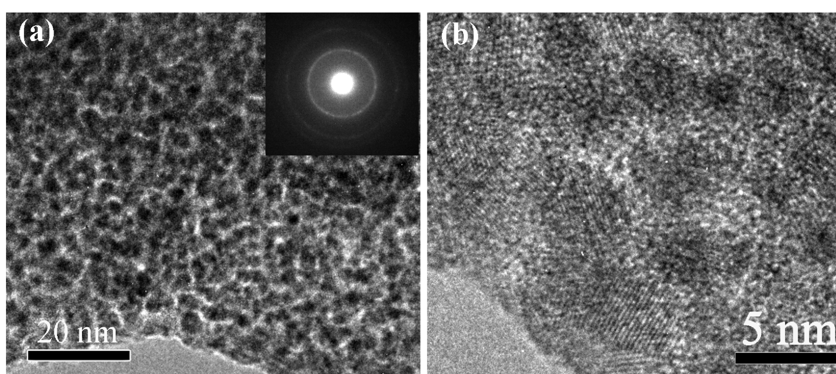

Figure 3 Plan-view TEM images for the sample in Fig. 2a: (a) low-magnification and (b) high-resolution. The inset shows the corresponding SAED pattern of the nanocrystalline silicon film.

© 2014 WILEY-VCH Verlag GmbH & Co. KGaA, Weinheim

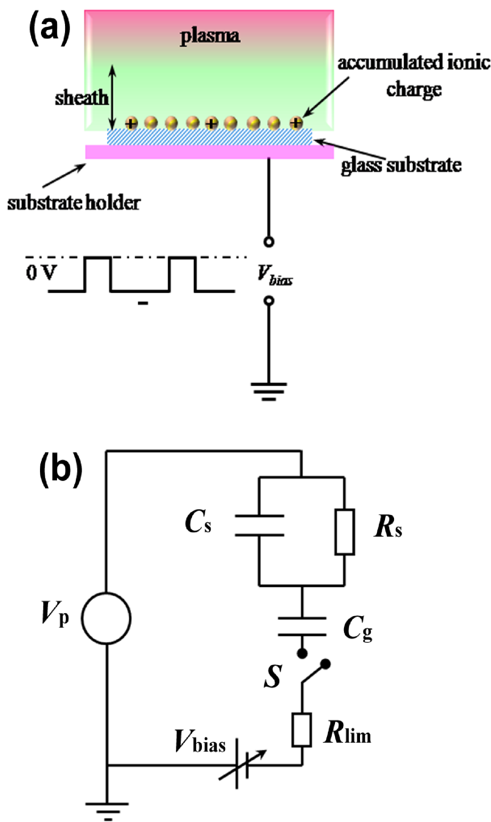

Figure 4 Schematic diagram of the biased glass substrate in a glow plasma (a) and the corresponding equivalent circuit (b).

deposited under a floating potential (in Fig. 2a). In the low-resolution TEM image (Fig. 3a), it can be observed that numerous small crystalline clusters with boundaries are randomly dispersed in the film. The inset of Fig. 3a shows the corresponding selected area electron diffraction (SAED) pattern of the nc-Si film. The spotty rings confirmed that the film consists of mixtures in which Si nanocrystals are embedded in amorphous silicon matrix. The high-resolution TEM image shown in Fig. 3b presents that the Si clusters compose of several small-sized nanocrystals (sub-5 nm). Combining the microstructure observation with the Raman analysis in Fig. 2h, it is speculated that the Si nanorods in Fig. 2g could be composed of a two-phase mixture of amorphous and nanocrystalline Si.

In order to get an in-depth understanding, a quantitative analysis was made to describe the charge/discharge processes of the glass capacitor during a pulse cycle. Figure 4a and b presents the sketched model of the above-mentioned capacitor and the corresponding equivalent circuit, respectively. Herein, the plasma is regarded as a low impedance voltage source V_p. R_s is the sheath resistance in parallel with the sheath capacitance C_s, meanwhile C_g is the parasitic capacitance of the glass substrate. In the equivalent circuit, we have neglected the internal impedance of the pulsed DC bias V_{bias}. R_{lim} ($=100\,\Omega$) is the current limiting resistance located between the biasing power supply and the substrate heater. Moreover, the sheath, located in between the plasma and the grounded wall, was also ignored. Without considering the edge effects, the capacitance is $C=\varepsilon\varepsilon_0 A/d$ for a parallel plate capacitor, where ε and ε_0 are the relative and vacuum permittivity, respectively, A is the area of the plates, and d the thickness of the dielectric medium. The vacuum permittivity ε_0 is equal to $8.85\times10^{-12}\,\mathrm{F\,m^{-1}}$. In the present case, the dielectric is the glass substrate with a thickness of $d=1\times10^{-3}$ m and a plate area of $A=7.5\times10^{-4}\,\mathrm{m^2}$. In view of effects of temperature and high-frequency electric field, we assume that the relative permittivity ε is 50 on the basis of the study in Ref. [14]. Thus, the parasitic capacitance C_g is $\sim3.3\times10^{-10}$ F. Before the bias V_{bias} is loaded, the surface of the glass capacitor accumulates electron charge from the plasma and develops a negative potential, namely, the floating potential (V_f). When the unipolar pulsed bias of -60 V (for the sample in Fig. 2c) is applied, the surface plate, initially at V_f -60, is charged toward positive following an exponential law (V_f $-60e^{-t/\tau}$) during the pulse-on phase, where t is the charging time. The charging speed of the glass capacitor depends on the time constant τ, which can be written as

$$\tau = C_g R_{eq} = C_g\left(R_{lim} + \frac{-j(R_s/2\pi f C_s)}{R_s - j(1/2\pi f C_s)}\right). \qquad (2)$$

In our experimental, the frequency f is 40 kHz for the MF magnetron power supply. Further, in light of investigations on a 100 kHz pulsed magnetron plasma [15], the equivalent sheath impedance $[-jR_s/(2\pi f C_s)]/[R_s - j/(2\pi f C_s)]$ is estimated to be 300 kΩ. In addition, it was reported that electrode sheathes generally present a pure resistive characteristic for low-frequency magnetron plasma [16]. Therefore, we should neglect the influence of the displacement current through the sheath capacitor C_s on the charge/discharge processes of the glass capacitor. The time constant for our case is calculated to be around 1×10^{-4} s. At the end of the pulse on time, the transient potential of the surface plate increased to V_f -31. It is clear that the surface plate can sustain a negative potential throughout the pulse-on phase, which is beneficial for extracting positive ions from the plasma. Next, during the pulse-off period, the surface plate obtains a potential more positive than V_f, and the accumulated ionic charge is neutralized through the electron flow from plasma. The surface plate returns to the floating potential when the pulse cycle is finished. To sum up, the potential of the growing surface experiences the aforementioned periodic change, thus leading to periodic ion bombardment (tens of eV) during the whole deposition process.

In general, the magnitude of the negative bias utilized has an important effect on modifying the microstructure of thin films. Comparing the SEM images presented in Figs. 2d, 5a and b (corresponding to -60, -20, and -90 V), we can conclude that increasing the negative voltage of the bipolar pulsed bias enables to promote formation of the agglomerate structure, namely, the growth of Si nanorods. This was confirmed by the cross-sectional images, as

© 2014 WILEY-VCH Verlag GmbH & Co. KGaA, Weinheim

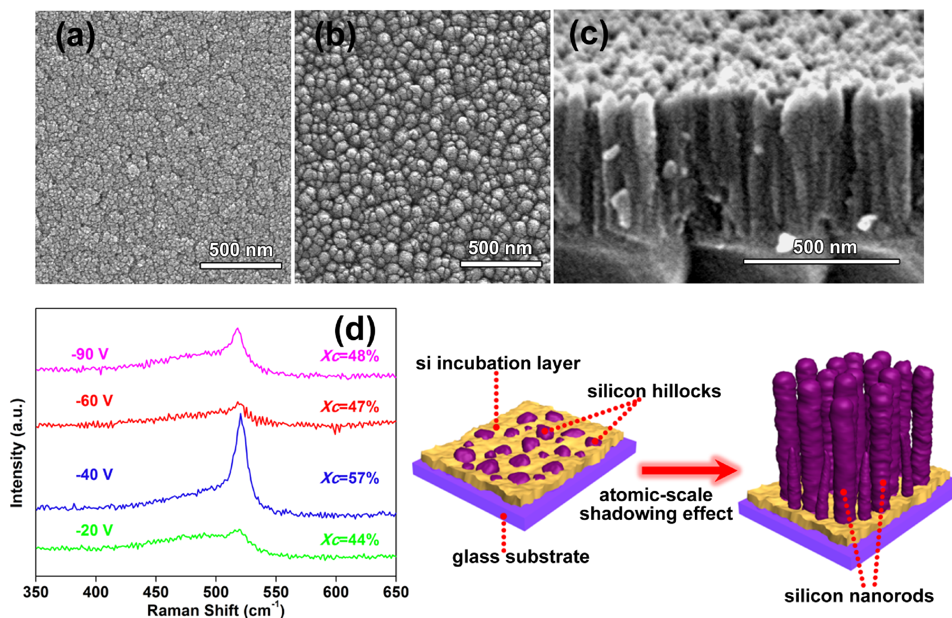

Figure 5 Top-views of the crystalline Si samples fabricated under different bias conditions (a) −20 V, (b) −90 V, and (d) their Raman spectra; (c) the cross-sectional view of the sample deposited at −90 V. Schematic illustrations of the silicon nanorod growth mechanism shown at the bottom right of the figure.

illuminated in Figs. 2g and 5c. The average diameter of the nanocrystalline Si nanorods is about 75 nm at −90 V, bigger than that of the −60 V case (shown in Fig. 2g). Higher negative bias voltage usually brings about more intensive ion bombardment onto the surface, resultantly enhancing the mobility of the deposited species. Figure 5d presents the Raman spectra of nanocrystalline Si films prepared at different negative voltages under bipolar-pulsed bias operating mode. In the case of −40 V, a crystalline volume fraction as high as ~57% was obtained. It was revealed that the optimum ion-bombardment is good for obtaining well-ordered structure, consistent with the previous studies [17, 18]. Based on the results revealed in Figs. 2 and 5, the growth mechanism of the Si nanorods on glass substrates was proposed, as illustrated at the bottom right of Fig. 5. Generally, due to high surface quality of the substrate, there is an incubation layer at the initial stage of the sputtering deposition [19], as revealed in Fig. 2f. During the initial phase, the nucleation, growth, and agglomeration of silicon clusters dominate over the growth behavior due to the enhanced adatom mobility using pulsed bias, which leads to the gradual coarsening of the growing surface. After the incubation period, numerous silicon hillocks with random distribution are created for the coming growth of silicon nanorods. Afterwards, the hillocks act as shadows to nearby areas, resulting in preferential growth on the hillock surfaces. Therefore, the head of the hillock captures most of the sputtering species and then grow up to be well-defined vertical nanorod. It is well known that some kinds of semiconductor nanorods arrays, such as TiO_2 [20] and ZnO [21], were fabricated by using self-organized porous alumina membrane masks. Due to the shadowing masks, these arrays possessed more uniform size and spacing than those of the Si nanorod arrays in our experiments. Moreover, Ding et al. [22] have fabricated highly ordered nanocrystalline Si:H nanodots on Si substrates by combining plasma-enhanced CVD with an alumina template-based fabrication approach. However, it is difficult to prepare Si nanorod arrays through the above template approach because of the high-aspect-ratio of the nanopores in the alumina membrane mask. In comparison, nanocrystalline Si nanorod arrays can be prepared conveniently by the MF magnetron sputtering method as proposed in this study.

Ultra-thin stainless-steel is usually used as a kind of flexible substrate in the modern optoelectronic devices. Figure 6a exhibits the side-view of the nanocrystalline Si nanorods prepared on stainless steel at 550 °C with a negative bipolar pulsed bias voltage of −32 V. The deposition conditions are the same as those of glass substrates, except for the substrate temperature and the bias voltage. The well-aligned vertical nanorods with an average diameter of ~80 nm are obtained, as seen in Fig. 6a. XRD measurements were performed to investigate the phase structure of nanocrystalline Si nanorods deposited on different substrates, as shown in Fig. 6b. The diffraction peaks corresponding to (111), (220), and (311) crystal planes of Si were clearly observed. The weak and broad peak features imply that the Si nanorods are composed of amorphous and nanocrystalline mixed-phase in our experiments. Furthermore, there are considerable discrepancies on the preferential orientation of the Si nanostructure deposited on glass or stainless steel substrate. Consequently, it is elucidated that the substrate nature has a distinct effect on the growth behavior of silicon nanocrystals, as reported by Ref. [23].

© 2014 WILEY-VCH Verlag GmbH & Co. KGaA, Weinheim

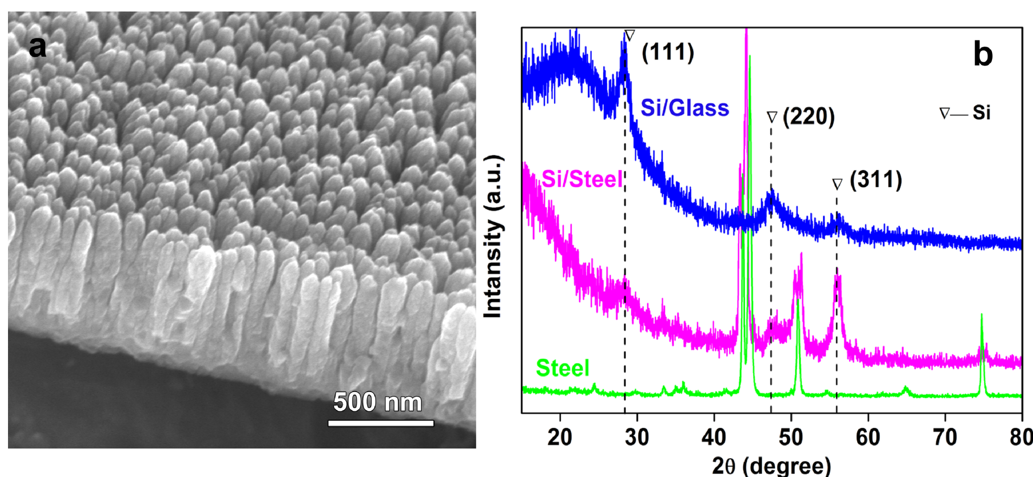

Figure 6 (a) Side-view of the Si nanorod film on the stainless steel prepared at 550 °C with a negative bias voltage of −32 V and (b) XRD patterns of Si nanorod films deposited on glass or steel substrates. The XRD pattern of the steel substrate is also depicted as a control.

4 Conclusions In conclusion, directional nc-Si nanorod array was successfully fabricated on the glass or stainless steel by MF magnetron sputtering technique with high deposition rate. During the deposition, the ion-bombardment conditions could be modified by changing pulsed DC bias, further demonstrating that the microstructure of nc-Si nanorods could be tailored by the pulsed bias. The bipolar pulsed bias was more efficient to enhance atomic transport on the growing surface, giving rise to the formation of Si nanorods. Well-aligned nanocrystalline Si nanorod array with a crystalline volume fraction of around 47% was achieved under a bipolar-pulsed bias with a frequency of 10 kHz, in which the negative bias voltages are ranging from −60 to −90 V. Furthermore, the successful preparation of nanocrystalline Si nanorod array on the stainless steel was also presented.

Acknowledgements The authors are grateful to the financial support by the National Nature Science Foundation of China (Grant No. 51302277 and 51102187), the Applied Research Funds for Public Welfare Project of Zhejiang Province (Grant No. 2014C31148), the Ningbo Nature Science Foundation (Grant No. 2013A610073), and the Project funded by China Postdoctoral Science Foundation.

References

[1] Q. J. Cheng, S. Y. Xu, and K. K. Ostrikov, J. Mater. Chem. **19**, 5134 (2009).
[2] J. Sanz-Robinson, W. Rieutort-Louis, Y. Z. Hu, L. H. Huang, N. Verma, S. Wagner, and J. C. Sturm, IEEE Electron Device Lett. **35**, 425 (2014).
[3] S. Guha, J. Yang, and B. J. Yan, Sol. Energy Mater. Sol. Cells **119**, 1 (2013).
[4] B. Z. Tian, X. L. Zheng, T. J. Kempa, Y. Fang, N. F. Yu, G. H. Yu, J. L. Huang, and C. M. Lieber, Nature **449**, 885 (2007).
[5] B. M. Kayes, H. A. Atwater, and N. S. Lewis, J. Appl. Phys. **97**, 114302 (2005).
[6] Y. J. Yu, C. Yue, S. B. Sun, W. Lin, H. Su, B. B. Xu, J. T. Li, S. T. Wu, J. Li, and J. Y. Kang, ACS Appl. Mater. Interfaces **6**, 5884 (2014).
[7] J. G. Fan and Y. P. Zhao, Nanotechnology **19**, 155707 (2008).
[8] Y. P. Zhao, D. X. Ye, G. C. Wang, and T. M. Lu, Nano Lett. **2**, 351 (2002).
[9] Y. H. Ma, F. Z. Liu, M. F. Zhu, J. L. Liu, H. H. Wang, Y. Yang, and Y. F. Li, Nanotechnology **20**(27), 275201 (2009).
[10] J. H. Gao, L. Zhang, J. Q. Xiao, J. Gong, C. Sun, and L. S. Wen, Mater. Lett. **68**, 367 (2012).
[11] A. Tabata, K. Fukaya, and T. Mizutani, Vacuum **82**, 777 (2008).
[12] E. Barnat and T. M. Lu, J. Vac. Sci. Technol. A **17**, 3322 (1999).
[13] P. J. Kelly and R. D. Arnell, Vacuum **56**, 159 (2000).
[14] C. Kim and M. Tomozawa, J. Am. Ceram. Soc. **59**, 127 (1976).
[15] S. K. Karkari, A. Vetushka, and J. W. Bradley, J. Vac. Sci. Technol. A **21**, L28 (2003).
[16] M. A. Lieberman and A. J. Lichtenberg (eds.), Principles of Plasma Discharges and Materials Processing (John Wiley & Sons, New York, 2005).
[17] F. Fenske, P. Reinig, B. Selle, and W. Fuhs, Surf. Coat. Technol. **174**, 801 (2003).
[18] N. Kosku, H. Murakami, S. Higashi, and S. Miyazaki, Appl. Surf. Sci. **244**, 39 (2005).
[19] S. Mukherjee and D. Gall, Appl. Phys. Lett. **95**, 173106 (2009).
[20] M. S. Sander, M. J. Côté, W. Gu, B. M. Kile, and C. P. Tripp, Adv. Mater. **16**, 2052 (2004).
[21] Q. T. Wang, G. Z. Wang, B. Xu, J. S. Jie, X. H. Han, G. P. Li, Q. S. Li, and J. G. Hou, Mater. Lett. **59**, 1378 (2005).
[22] G. Q. Ding, W. Z. Shen, M. J. Zheng, W. L. Xu, Y. L. He, and Q. X. Guo, J. Cryst. Growth **283**, 339 (2005).
[23] M. Kondo, Y. Toyoshima, and A. Matsuda, J. Appl. Phys. **80**, 6061 (1996).

© 2014 WILEY-VCH Verlag GmbH & Co. KGaA, Weinheim